A $LaBr_3$:Ce Fast-timing Array for DESPEC at FAIR

O.J. Roberts[a], A.M. Bruce[a], P.H. Regan[b,e], Zs. Podolyák[b], C.M. Townsley[b], J.F. Smith[c], K.F. Mulholland[c], A. Smith[d]

[a] *School of Computing, Engineering and Mathematics, University of Brighton, Brighton BN2 4GJ, UK.*
[b] *Department of Physics, University of Surrey, Guildford GU2 7XH, UK.*
[c] *School of Engineering, The University of the West of Scotland, Paisley PA1 2BE, UK.*
[d] *The University of Manchester, Oxford Road, Manchester, M13 9PL, UK.*
[e] *National Physics Laboratory, Teddington, TW11 0LW, UK.*

Abstract

The design of a fast-timing γ-ray detection array aimed at measuring sub-nanosecond half-lives using $LaBr_3$:Ce scintillation crystals is presented. This array will complement novel and existing charged particle and neutron detector arrays at the low-energy branch of a fragment separator (Super-FRS), to be built within the NuSTAR collaboration as part of the future Facility for Anti-proton and Ion Research (FAIR). The array will be used in conjunction with the Advanced Implantation Detector Array (AIDA), to measure implant-decay correlations. Monte-Carlo simulations have been performed to determine the design of the proposed fast-timing array around a localised implantation point. In particular, simulations were used to determine the full-energy peak efficiencies for single cylindrical, conical and 'hybrid' detector geometries, as well as complete array configurations of 'hybrid' and ø1.5"x2" cylindrical crystals. Timing precision calculations were then used to determine the timing response for each configuration based on its simulated efficiency. An informed decision based on the simulated efficiencies and timing precision calculations allowed the optimum configuration for the array to be determined.

Keywords: GEANT4, $LaBr_3$:Ce, DESPEC, FAIR, AIDA, Fast-timing

1. Introduction

The development of a new synchrotron and an in-flight separator (Super-FRS) [1] at FAIR [2] will deliver a large number of rare isotopes, which will allow the study of very short-lived nuclei at the extremes of existence. The Nuclear STructure, Astrophysics and Reactions (NuSTAR) [3] international collaboration was established to develop and equip this facility with nine experimental set-ups which include, HIgh-resolution in-flight SPECtroscopy and DEcay SPECtroscopy (HISPEC/DESPEC) [4–7]. The combination of a higher primary beam intensity and the Super-FRS will allow access to nuclei along the rapid-neutron capture process (r-process) path in neutron-rich nuclei where a

Email address: O.J.Roberts@brighton.ac.uk (O.J. Roberts)

'stopped beam' set-up of charged particle, γ-ray and neutron detectors can be utilised at the focal point of the low-energy branch of the Super-FRS [8].

Decay spectroscopy usually involves the implantation of ions from the separator into an 'active catcher' of highly segmented double-sided silicon-strip detectors (DSSDs), (eg. refs. [9, 10]). After the ions are implanted they β-decay (or α-decay), releasing additional energy in the form of γ rays and internal conversion electrons. The high pixellation of these silicon detectors allows the correlation of the time and position of the implantation of the heavy ion, with the signal produced in the same detector from the subsequent β-decay. It is envisaged that AIDA [11], an implantation array formed of 20 DSSDs each with an area of 8x8 cm and a thickness of 1 mm [11], will be used to make these implant-decay correlations. It will be complemented by the addition of an array of germanium detectors, or of neutron detectors, such as the MOdular Neutron SpectromeTER (MONSTER) [12], or the BEta-deLayEd Neutron detector (BELEN) [13] for cases where the β^--decay populates excited states in the daughter nucleus that lie above the neutron separation energy for that system, a phenomenon observed in neutron-rich nuclei [14, 15]. This paper presents details of possible configurations for a fast-timing array to be used with AIDA to measure half-lives of excited states in exotic nuclei.

In preparation for the UK array, $LaBr_3$:Ce detectors have been used to augment existing high-purity germanium (HpGe) arrays at the IFIN-HH, ILL and RIKEN laboratories. Such mixed arrays have been successful in measuring sub-nanosecond half-lives of excited states (i.e. $T_{\frac{1}{2}}$>50 ps) using $\gamma\gamma$ coincidences [16–22]. At RIKEN, the half-life of the yrast 2^+ state in ^{104}Zr has been re-measured using $\beta\gamma$ coincidences with the β-timing coming from fast plastic scintillators at the front and back of the WAS3ABi (Wide-range Active Silicon-Strip Stopper Array for β and Ion detection) detector. The measured value was found to be in good agreement with the literature value of 2.0(3) ns [23]. The current design of AIDA does not have fast plastic scintillators so the timing resolution of such a setup would be strongly influenced by the timing resolution of the silicon-strip detectors in AIDA, expected to be several nanoseconds [24]. This would provide the limit on the $T_{1/2}$ measured in $\beta\gamma$ mode.

The half-life of an excited state is typically measured by taking the time difference between the γ rays feeding and de-exciting the state of interest [25]. In cases where the half-life is sufficiently short that an exponential tail cannot be fitted to the slope of the observed decay, the centroid shift method is used [18, 26–28]. In this method, the half-life is extracted from time spectra obtained by imposing gates on the measured energies. After the time-walk and Compton corrections have been performed [16, 17, 25, 28–30], the time associated with the feeding γ-ray of energy E_{γ_1}, and de-exciting γ-ray with energy E_{γ_2} is the forward time spectrum, $\Delta T = T_1$-T_2, where T_1 and T_2 are the times related to γ rays γ_1 and γ_2 respectively. The time for the reverse situation (E_{γ_2},E_{γ_1}) is $\Delta T = T_2$-T_1. The mean-life can be extracted from the difference between the centroids of the two gated time spectra.

Over the past 15 years, there has been development of high resolution scintillators for γ-ray spectroscopy. Traditionally, BaF_2 crystals were used for timing due to their fast response, however they have poor energy resolution ($\Delta E/E \sim 9$ % at 662 keV [31, 32]). One of the most notable inorganic scintillators to emerge is cerium doped lanthanum tri-bromide ($LaBr_3$:Ce). Doping the $LaBr_3$ crystals with Ce^{3+} produces luminescence in the blue/UV part of the electromagnetic spectrum (λ_{max} = 380 nm) [33], compatible

with modern photo-multiplier tubes (PMTs). The timing response of $LaBr_3$:Ce depends on the concentration of Ce^{3+} [34]. The timing resolutions at full-width half maximum (FWHM) for ^{60}Co peak-to-peak coincidences in a ø1″x1″ crystal have been reported to be ~150 ps [16] (coincidence resolving time, CRT), and 107(4) ps [35] (individual timing resolution) with $LaBr_3$:Ce scintillators doped with 5 % of Ce^{3+}. $LaBr_3$:Ce has a typical energy resolution of ~ 3 % (FWHM) at 662 keV [7, 19, 33], which is significantly better than BaF_2. Also, the additional stopping power of the scintillator (due to its high density of 5.07 g/cm^3 [33]), means that it has much better efficiency per unit volume than NaI:Tl. Therefore, $LaBr_3$:Ce is a desirable material to use for γ-ray spectroscopy and for measuring sub-nanosecond half-lives.

2. Design Criteria for the Array

In order to fulfil its intended purpose, the fast-timing array needs to be both modular and efficient, covering as much of the solid angle as possible. In addition, the crystals need to be large enough to detect γ-ray photons up to ~ 4 MeV, for discrete measurements associated with core-breaking decays in the region of magic or semi-magic nuclei [36, 37]. However, since the intrinsic timing resolution increases with increasing crystal size, a balance between the detector efficiency and timing resolution needs to be reached. Monte-Carlo simulations using GEANT4 [38] were used to help identify the optimal size, shape, and arrangement of $LaBr_3$:Ce detectors. The simulations were validated by comparing the efficiencies calculated using GEANT4 for the array of 11 $LaBr_3$:Ce detectors at Bucharest, with the values measured for ^{152}Eu. Good agreement between the two was reached.

Cylindrical crystals with dimensions; ø1″x1″, ø1.5″x1.5″, ø1.5″x2″ and ø2″x2″ were considered and compared with two novel geometrical designs which have been shown for BaF_2 crystals to reduce the time spread associated with the scintillation collection process [32]. These novel geometrical designs are a conical crystal and a conical-cylindrical 'hybrid' design defined as a truncated cone attached to a cylinder, as shown in figure 1. The conical crystals have front and back window diameters of 1″ and 1.5″ respectively, and a length of 1.5″.

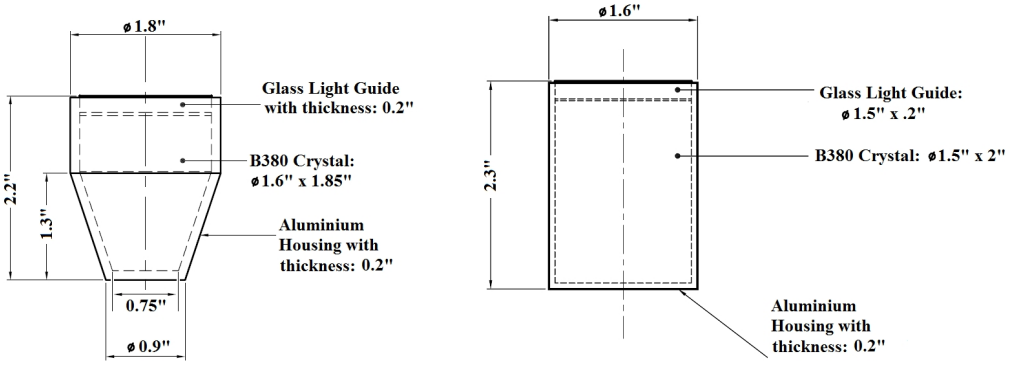

Figure 1: The size of the $LaBr_3$:Ce crystal, aluminium housing and light guide for:(left), the 'hybrid' and (right), the ø1.5″x2″ crystals. B380 is the brand name of the crystal.

The minimum radius for which an integer number of each detector type could be tiled in a ring around AIDA [11] was calculated. The centre of the tenth DSSD was chosen as the implantation point and treated as an isotropic point source. The simulation included the aluminium can of dimensions 10x10x50 cm and thickness of 2 mm. The distance from the implantation point to the corners of the can is 7.07 cm. A radius of 8.3 cm was determined to give an integer number of all the proposed detector sizes. The number of each detector type needed in one ring around AIDA is presented in table 1 along with their typical CRTs, which is influenced by the size of the crystal, the type of photo-sensor, the response of the timing electronics and γ ray energy.

#	Dimensions	Geometry	T_{FWHM} at 511 keV	T_{FWHM} at 1332 keV
8	ø2″x2″	Cylindrical	450 [39]	300 [16]
10	ø1.5″x2″	Cylindrical	400	210
10	ø1.5″x1.5″	Cylindrical	360 [39]	180 [16]
13	ø1″x1″	Cylindrical	200 [29]	150 [16, 35, 40]
13	ø1″x1.5″xø1.5″	Conical	-	160 [40]
13	ø0.75″x1.85*″xø1.5″	Hybrid	-	-

Table 1: The number of each crystal type that is needed to construct a ring around AIDA with R=8.3 cm is shown in the first column. The length quoted for the 'hybrid' (*) geometry is the total crystal length (i.e. conical plus cylindrical sections). The last three columns contain the type of crystal geometry and reported CRTs in picoseconds. The values for the ø1.5″x2″ crystals were measured using Hamamatsu H10570 PMTs. Timing resolution values for the 'hybrid' detectors are not available.

2.1. The Simulated Detector Efficiency

The isotropic point source located at the centre of the ring emitted 10^6 simulated γ-ray events at energies ranging between 100 and 4000 keV at intervals of 100 keV up to 1 MeV and then at intervals of 500 keV from 1 to 4 MeV. Figure 2 shows the simulated energy spectra of a ring of 12, ø1.5″x2″ detectors for energies of 500, 1000, 2000 and 4000 keV and energy resolutions (FWHM) were determined using the formula [41]:

$$\frac{FWHM}{E} = a \cdot E_{\gamma}^{-\frac{1}{2}} \tag{1}$$

where a is calculated to reproduce the energy resolution (FWHM) of 3.3 %, measured in the current work, for a γ-ray energy (E_γ) of 662 keV for a ø1.5″x2″ crystal.

Figure 3 shows the full-energy peak efficiencies for one ring of each of the detector types listed in table 1, with the 50-550 keV region expanded for clarity to the right of the figure. For $E_\gamma \geq$ 200 keV, the ring of 13 'hybrid' crystals has the highest efficiency. As a ø2″x2″ crystal has the largest volume of all the simulated crystals, it might be expected to have the highest full-energy peak efficiency. However when it is tiled around the implantation point, the lack of truncation at the front of these crystals results in an increased amount of dead space. Hence, there are only 8 cylinders but 13 'hybrid' crystals in one ring as shown in table 1. At E_γ = 500 keV and 1000 keV the full-energy peak

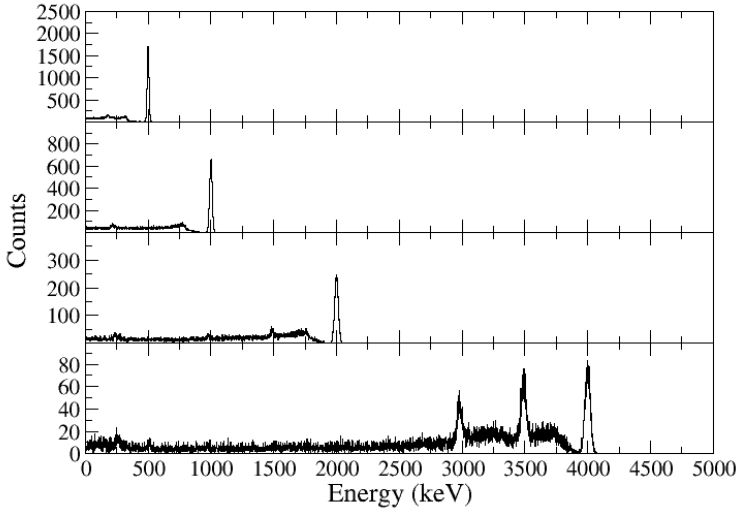

Figure 2: Simulated energy spectra of a ring of 12, ø1.5″x2″ crystals for γ-ray energies of 500 (top), 1000 (2^{nd} panel), 1500 (3^{rd} panel) and 4000 keV (bottom panel) respectively. The insulation and housing of the crystals were included in the simulations, using the quoted dimensions in figure 1. A thickness of 2 mm of lead shielding was also added[1]. The light guides behind the crystals were not included in the simulations. A total of 10^6 events were simulated for each energy.

efficiency of a ring of ø2″x2″ crystals is 6.8 and 3.1 % respectively, compared to 11.4 and 6.6 % respectively for a ring of 'hybrid' crystals. The full-energy peak efficiency of a ring of eight ø2″x2″ crystals is less than a ring of 'hybrid' crystals except for when $E_\gamma \leq$ 200 keV. At E_γ = 100 keV and 300 keV the full-energy peak efficiency of a ring of ø2″x2″ crystals is 18.5 and 11.5 % respectively, and 16.6 and 14.5 % respectively for a ring of 'hybrid' crystals. In this energy range, the ring of 'hybrid' crystals has an efficiency comparable to that of a ring ø1.5″x2″ crystals due to the small diameter (shown in figure 1) at the front of each detector. Figure 3 shows that a ring of eight ø1.5″x2″ crystals has the third highest full-energy peak efficiency (~ 5 % for E_γ = 500 keV) and that the peak efficiencies of the ø1″x1″, ø1.5″x1.5″ and conical crystals were lower than for the other configurations.

2.2. Timing Precisions

The precision of a half-life measurement depends on the timing resolution of the setup and the level of statistics (10^4 counts are needed in order to make a measurement to within an error of 1% assuming Poisson statistics). The coincidence timing precision

[1]There is flexibility in the design of the array to add an additional 5 mm of μ-metal to the existing 2 mm of shielding around each detector, before the detectors will need to be moved further back.

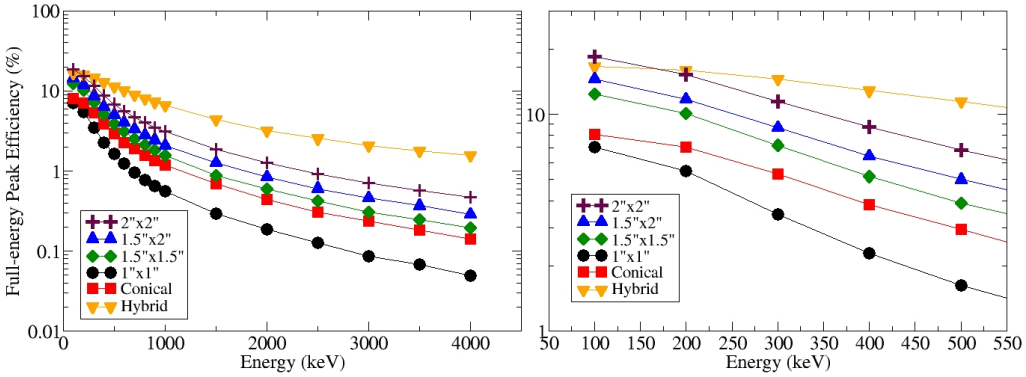

Figure 3: (Colour on-line) Left: The simulated full-energy peak efficiencies of a ring of each detector type with a radius of 8.3 cm from the implantation point. Right: The same plot as in the left panel, but enlarged to show the details for $E_\gamma \leq 500$ keV. The statistical errors are smaller than the data points.

can be calculated using the efficiency and timing response [16, 42] of coincident detectors, defined by Mach et al. [43] as:

$$Timing\ \ Precision\ (TP) = \frac{T_{\mathrm{FWHM}}}{\sqrt{N}}, \tag{2}$$

where T_{FWHM} is the full-width half maximum (FWHM) of the timing response, and N is the total number of counts (coincidences) in the timing spectrum.

2.2.1. Coincidence Timing Precisions

Coincidence timing precisions were calculated using equation 2, the CRTs shown in table 1 and the calculated efficiencies shown in figure 3 for a ring of each size of detector. The coincidence timing precisions can also be obtained by using the individual detector efficiencies or scaling by the volume of the crystal size used. The results are presented in table 2 and are normalised to the ø1″x1″ detectors as this detector type has the best intrinsic timing resolution. The range of values for the conical detectors arises from scaling the measured T_{FWHM} at 1332 keV to 511 keV. Factors of 1.33 and 2 have been used to get the two extremes based on the measured values for the ø1″x1″ and ø1.5″x1.5″ cylindrical detectors, as listed in table 1. The timing precision values for a ring of 'hybrid' detectors were calculated using the CRTs of the ø1.5″x2″ detectors. Since no data on the timing resolutions at 4000 keV is available, the simulated efficiencies at 4000 keV and the CRT of each detector at 1332 keV were used to get an approximate value for the timing precision at 4000 keV.

Table 2 shows that the ø2″x2″ and ø1.5″x2″ detectors are approximately a factor of 2 better than the ø1″x1″ detectors at 511 keV and about 3 times better at 1332 keV. This is

[2]This range has been calculated by scaling the measured T_{FWHM} at 1332 keV to 511 keV (see text for details).

Coincidence mode			
Detector size	TP at 511 keV	TP at 1332 keV	TP at 4000 keV
ø2″x2″	0.53	0.34	0.21
ø1.5″x2″	0.64	0.39	0.24
ø1.5″x1.5″	0.74	0.41	0.30
ø1″x1″	1.00	1.00	1.00
Conical (ø1″x1.5″xø1.5″)	0.57-0.87[2]	0.44	0.37
Hybrid (ø0.75″x1.85″xø1.5″)	0.28	0.10	0.04

Table 2: The coincidence timing precisions (TP) normalised to the values for the ø1″x1″ crystals. The precisions at 4000 keV were calculated using the simulated full-energy peak efficiencies at 4000 keV from GEANT4 along with the CRTs at 1332 keV.

because the gain in efficiency from using these detectors outweighs their poorer intrinsic timing resolution. At the higher energy of 4 MeV, the difference in efficiency between the different crystals becomes more pronounced and table 2 shows that the ø1″x1″ and conical detectors would be factors of ~ 5 and ~ 2 worse than the ø2″x2″ detectors at this energy respectively.

2.3. The Full array Configuration

The simulated efficiencies shown in section 2.1 and the results of calculating the timing precisions discussed in section 2.2, allow us to make an informed decision about which detectors to include in the full-array simulations.

The relative timing precisions of the ø1″x1″ and conical detectors at 4 MeV indicate that they would not be a good choice for measuring efficiently at high energy. Therefore both of these detector geometries were not considered further. The ø1.5″x1.5″ detectors were ruled out in favour of the extra full-energy peak efficiency, and better timing precisions offered by the ø2″x2″ and ø1.5″x2″ detectors. Table 2 shows the ø2″x2″ detectors have a similar timing precision in coincidence mode to the ø1.5″x2″ detectors, and thus the slightly smaller ø1.5″x2″ detectors were chosen in order that the system remained as modular as possible, and to minimise costs. This leaves two types of detector for further consideration; the 'hybrid' and ø1.5″x2″ detectors. The results of simulating various full array configurations using these detector types will now be discussed.

A variety of configurations of up to 36 detectors in three rings around the AIDA implantation point were considered, including a cross configuration with supplemental detectors at 45°, a cross configuration of detector clusters around AIDA, and a conventional 'ball' (as shown in figure 4). The full-energy peak efficiencies from these simulations for multiplicity one γ rays up to 4 MeV, are shown in figure 5. These simulations included 2 mm of lead shielding around each of the detectors, which serve to reduce the amount of Compton scattering between adjacent crystals and increase the peak-to-background ratio.

Figure 5 shows that for both 36 detector array configurations, the 'hybrid' detector array has a higher full-energy peak efficiency than the ø1.5″x2″ cylindrical detector array over the full energy range. Two variations of the cross configuration (four 2x3 clusters of 24 detectors, and two 2x3 clusters plus two 3x3 clusters of 30 detectors), were also simulated with ø1.5″x2″ crystals. Both of these designs were found to have a

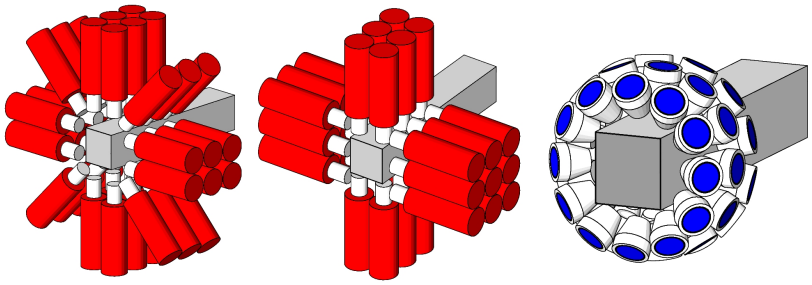

Figure 4: (Colour on-line) Left: The 'cross' configuration with supplemental detectors at 45° in 3 rings, consisting of 36 ø1.5″x2″ detectors. Centre: The 'cross' configuration of 30 ø1.5″x2″ detectors in 3x3 and 2x3 clusters. Right: A spherical array of 36 'hybrid' detectors, shown without the PMTs.

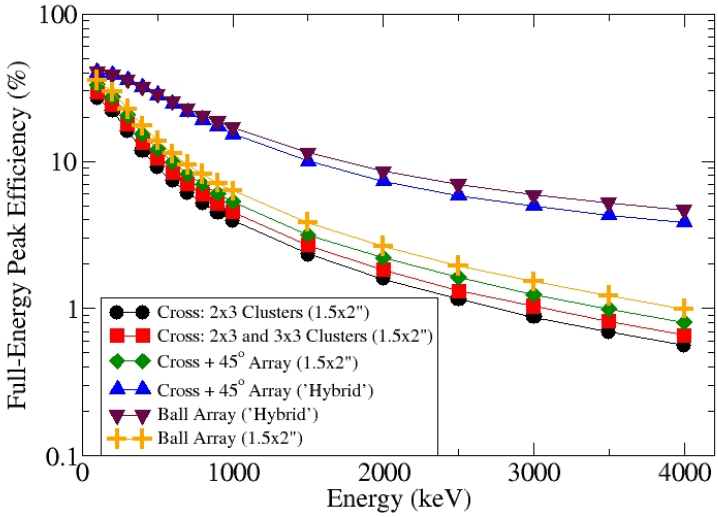

Figure 5: (Colour on-line) The simulated full-energy peak efficiencies of the 'hybrid' and ø1.5″x2″ detectors in the proposed configurations of the array; 24 and 30 detectors in the 2x3 and 2x3 plus 3x3 cluster cross arrangements respectively, and 36 detectors in the 'cross + 45°' and 'ball' set-ups. The statistical errors are smaller than the data points.

poorer overall efficiency than the cross configuration with detectors at 45°, which is not unexpected since they contain fewer crystals.

Figure 5 also shows that the tapered fronts of the 'hybrid' detectors and their length of 1.85″ make them very efficient detectors when they are tiled into an array, as they can be moved closer to the implantation point. It will be interesting to discover the energy and timing characteristics of this design once they are readily available. They may be the

choice for future arrays, however given that they are still under development and that no firm data is currently available in the literature, the time constraints of the project prompted the decision to use the next best option, which is the ø1.5″x2″ cylindrical crystals.

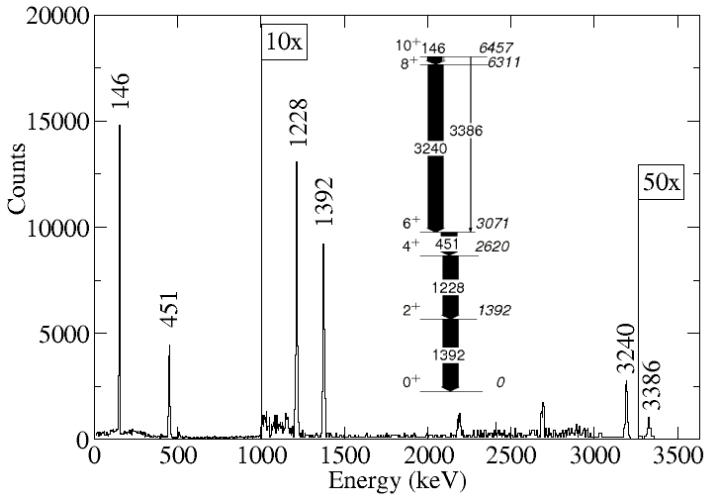

Figure 6: A simulated singles γ-ray energy spectrum showing transitions below the 10^+ isomer in ^{54}Ni [36], generated from a single point source in the middle of AIDA. The simulation includes attenuation due to the vacuum box around the AIDA detectors, but not the self-activity within the $LaBr_3$:Ce crystals, lead x-rays or atomic background.

Figure 6 shows a simulated singles γ-ray energy spectrum displaying the response of 36, ø1.5″x2″ $LaBr_3$:Ce crystals in the cross configuration with detectors at 45°, to transitions below the $I^{\pi}=10^+$ isomer in ^{54}Ni, which are seen very clearly in the spectrum. The simulated events emanated isotropically from a source at the centre of the array. The level of statistics (4.8 x 10^6 events) and branching ratios (5% 3386 keV, 94% 146 keV), were taken from Ref. [36]. The internal conversion of the 146 keV transition was determined using BRICC [44] and also included in the simulation.

3. Conclusions and Outlook

The Monte-Carlo simulation package GEANT4 was used to determine the full-energy peak efficiencies for different arrangements of a variety of shapes and sizes of $LaBr_3$:Ce crystals over an energy range from 0.1 to 4 MeV. The coincidence resolving times (CRTs) of the crystals taken from the literature were then combined with the efficiencies obtained from the GEANT4 simulations to derive an energy-dependent timing precision. Based on these calculations the ø1.5″x2″ and 'hybrid' detectors were selected to be tiled into different configurations, which included a modular arrangement of three rings of 12 detectors, as well as a conventional 'ball' set-up. Their simulated full-energy peak efficiencies were then compared in section 2.3, figure 5. The uncertainty in the timing response and energy resolution of the 'hybrid' detectors and the time constraints of the

project resulted in the purchase of the ø1.5″x2″ cylindrical detectors. Future work will focus on the effect that a distributed source of γ rays will have on the precision that can be obtained.

4. Acknowledgments

This project was funded by the UK NuSTAR grant from the Science and Technology Facilities Council (STFC). The authors would like to thank the FATIMA and DESPEC collaborations for feedback on this work.

References

[1] H. Geissel et al. *Nucl. Instr. Methods B 204, 71,* 2003.
[2] Green Paper - The Modularized Start Version, *http://www.fair-center.eu/fileadmin/fair/publications* October, 2009.
[3] FAIR Baseline Technical Report, *http://www.fair-center.eu/fileadmin/fair/publications_FAIR/FAIR_BTR_4.pdf*, March, 2006.
[4] Zs. Podolyák et al. *Nucl. Instr. Methods B 266, 4589,* 2008.
[5] B. Rubio. *Int. J. of Mod. Phys. E15, 1979,* 2006.
[6] Zs. Podolyák et al. *Int. J. of Mod. Phys. E15, 1967,* 2006.
[7] P.H. Regan et al. *Applied Radiation and Isotopes 70, 1125,* 2012.
[8] I. Dillmann et al. *Progress in Particle and Nuclear Physics 66, 2, 358,* April, 2011.
[9] N. Alkhomashi et al. *Phys. Rev. C 80, 064308,* 2009.
[10] N. Al-Dahan et al. *Phys. Rev. C 85, 034301,* 2012.
[11] T. Davinson et al. *Technical Report for the Design, Construction and Commissioning of the Advanced Implantation Detector Array (AIDA)* , November 2008.
[12] A.R. Garcia et al. *JINST 7, 05012,* 2012.
[13] M.B. Gomez-Hornillos et al. *J. Phys.: Conf. Ser. 312, 052008,* 2011.
[14] F.K. Thieleman et al. *Z. Phys. A 309, 4, 301,* 1983.
[15] R.E. Azuma et al. *Phys. Rev. Lett. 43, 1652,* 1979.
[16] N. Mărginean et al. *Eur. Phys. J A 46, 329,* 2010.
[17] J.-M. Régis et al. *Nucl. Instr. Methods A 726, 191,* 2013.
[18] T. Alharbi et al. *Phys. Rev. C 87, 014323,* 2013.
[19] T. Alharbi et al. *Applied Radiation and Isotopes 70, 1337,* 2012.
[20] P.J.R. Mason et al. *Phys. Rev. C 88, 044301,* 2013.
[21] S. Kisyov et al. *J. Phys.:Conf. Ser. 366, 012027,* 2012.
[22] S. Kisyov et al. *Phys. Rev. C 84 014324,* 2011.
[23] J.K. Hwang et al. *Phys. Rev. C 73 044316,* 2006.
[24] T. Davinson, *Priv. Comm.*
[25] H. Mach et al. *Nucl. Instr. Methods A 280, 49,* 1989.
[26] W. Andrejtscheff et al. *Nucl. Instr. Methods A 204, 123,* 1982.
[27] P. Petkov et al. *Nucl. Instr. Methods A 321, 259,* 1992.
[28] H. Mach et al. *Nucl. Phys. A 523, 191,* 1991.
[29] J.-M. Régis et al. *Nucl. Instr. Methods A 622, 83,* 2010.
[30] J.-M. Régis et al. *Nucl. Instr. Methods A 684, 36,* 2012.
[31] L.M. Fraile et al. *Nucl. Instr. Methods A 701, 235,* 2013.
[32] H. Mach and L.M. Fraile *Hyperfine Interactions, In Press: DOI:10.1007/s10751-012-0613-8,* 2012.
[33] C.M. Rozsa, P.R. Menge and M.R. Mayhugh. *BrilLanCe 380 Scintillators Performance Summary,* 2009.
[34] K.S. Shah et al. *Preprint. LBNL, 51793,* 2008.
[35] M. Moszynski et al. *Nucl. Instr. Methods A 567, 1, 31,* 2006.
[36] D. Rudolph et al. *Phys. Rev. C 78, 021301,* 2008.
[37] M. Górska et al. *Phys. Lett. B 672, 313,* 2009.
[38] S. Agostinelli et al. *Nucl. Instr. Methods A 506, 250,* 2003.
[39] Saint-Gobain, *Scintillation Products Technical Note, BrilLanCe Scintillators Performance Summary, January,* 2009.

[40] L.M. Fraile et al. ISOLDE Workshop, Fast timing results at ISOLDE, November, 2009.
[41] M. Ciemala et al. *Nucl. Instr. Methods A 610, 1, 76,* 2008.
[42] I. Deloncle et al. *J. Phys.:Conf. Ser. 205,* 012044, 2010.
[43] H. Mach. The initial plans for a fast timing array at DESPEC, *http://nuclear.fis.ucm.es/fasttiming/files/*
[44] T. Kibédi et al. *Nucl. Instr. Methods A 608, 202,* 2009.